

# Substrate Release Mechanisms for Gas Metal Arc Weld 3D Aluminum Metal Printing

Amberlee S. Haselhuhn,<sup>1</sup> Eli J. Gooding,<sup>1</sup> Alexandra G. Glover,<sup>1</sup> Gerald C. Anzalone,<sup>1</sup> Bas Wijnen,<sup>1</sup> Paul G. Sanders,<sup>1</sup> and Joshua M. Pearce<sup>1,2</sup>

## Abstract

*Limited material options, prohibitively expensive equipment, and high production costs currently limit the ability of small and medium enterprises to use 3D printing to prototype and manufacture metallic goods. A low-cost open-source 3D metal printer that utilizes gas metal arc welding technology has been developed that could make metal printing accessible to the average consumer. Unfortunately, this technology would demand access to expensive cutting tools for part removal from the substrate. This article investigates several substrate treatments to provide a low-cost method to easily remove 3D-printed 1100 aluminum parts from a reusable substrate. Coatings of aluminum oxide and boron nitride on 1100 aluminum and A36 low-carbon steel substrates were tested. Lap shear tests were performed to assess the interlayer adhesion between the printed metal part and the print substrate. No warping of the substrate was observed during printing. It was determined that boron nitride-coated low-carbon steel provided the lowest adhesion strength. Printing aluminum on uncoated low-carbon steel also allowed easy removal of the aluminum part with the benefit of no additional coating steps or costs.*

## Introduction

3D PRINTING HAS the potential to revolutionize the way goods are manufactured on a global scale, enabling mass customization while reducing both capital investment and production costs.<sup>1,2,3,4</sup> The ability of small and medium enterprises (SMEs) to make full use of this potential is currently restricted by material choice. Most SMEs only have local access to polymeric fused filament fabrication (plastic material extrusion). Third-party prototyping services offer a broader range of print media, including ceramics and metals. Most commercial 3D metal printers are out of reach of SMEs as they typically cost more than \$500,000.

3D metal printing is commercially available in several forms: laser-based additive manufacturing, weld-based additive manufacturing, and shape deposition modeling. Laser-based additive manufacturing methods include powder bed fusion (direct metal laser sintering),<sup>5</sup> selective laser sintering,<sup>6</sup> selective laser melting,<sup>7</sup> and directed energy deposition (laser cladding).<sup>6</sup> These methods offer excellent dimensional control but have large production costs due to the use of lasers or metal powders.

Weld-based additive manufacturing methods include gas metal arc welding (GMAW),<sup>8,9</sup> gas tungsten arc welding,<sup>10</sup> directed energy deposition and powder bed fusion (electron beam melting),<sup>7</sup>

electron beam freeform fabrication,<sup>11</sup> and microwelding<sup>12,13</sup> in a single-layer multipass welding regime. Parts produced by weld-based additive manufacturing are inexpensive and nonporous with good interlayer adhesion, but have a limited print resolution and poor surface finish. Microwelding is the exception, exhibiting excellent dimensional control and finer surface finish resulting from the small-diameter electrode and wire employed.

Shape deposition manufacturing processes feature both additive and subtractive manufacturing.<sup>14,15,16</sup> A single layer of metal is melted, sintered, or welded in a rough net shape and then subsequently milled down to a precise geometry before the next layer of metal is

Departments of <sup>1</sup>Materials Science & Engineering and <sup>2</sup>Electrical & Computer Engineering, Michigan Technological University, Houghton, Michigan.

printed. These processes have excellent dimensional control but are expensive and time-consuming as both printing and computer numerical control (CNC) milling equipment are required to produce a part.

The high cost and slow throughput of the current commercial metal 3D printers limit their application to expensive finished products such as custom hip replacements and maxillofacial repairs.<sup>17</sup> There is thus an urgent need for a low-cost 3D printer capable of depositing metals directly for both rapid prototyping and rapid manufacturing for SMEs.

Recent development of a low-cost open-source 3D metal printer exploiting GMAW technology offers the potential for the general public to 3D print metal parts.<sup>18</sup> This printer, based on the RepRap concept<sup>19</sup> (self-replicating rapid prototyper), is capable of being partially manufactured either by itself or produced in an incremental fashion from components produced by a standard fused filament fabrication system. It utilizes a moving stage upon which the substrate is placed and a fixed print head comprised of a workshop GMAW. Aluminum and steel parts have been printed with this printer using single-pass, multilayer welding and were removed from the substrate with a vertical band saw. This method of part removal is suboptimal as it requires additional processing equipment, costs, and time. Thus, an alternative method is desired.

This article investigates several substrate treatments to provide low-cost release mechanisms to remove 3D-printed aluminum metal parts from the print substrate, outlined in Table 1. The substrate adhesion and strength of the

interface between the 3D-printed part and substrate was quantified using a lap shear measurement commonly employed to assess the strength of adhesives.<sup>20</sup> The results are discussed and a generalized mechanism is proposed for enabling substrate selection for aluminum GMAW 3D printing.

## Materials and Methods

### Description of a 3D Metal Printer

The metal printer comprised two distinct components, a workshop-grade gas

metal arc welder and a three-axis stage as shown in Figure 1.<sup>16</sup> The GMAW, a Millermatic 140 with Spoolmate 100 weld gun, supplied the material used to print and the energy required to melt the material. The three-axis stage was microprocessor controlled, permitting precise CNC of both the position and speed of the platform upon which parts were printed. The part was built upon a sacrificial 6.35-mm-thick mild steel or aluminum plate.

The stage was derived from an open-source 3D printer design known as a Rostock,<sup>21</sup> which is a RepRap derivative.

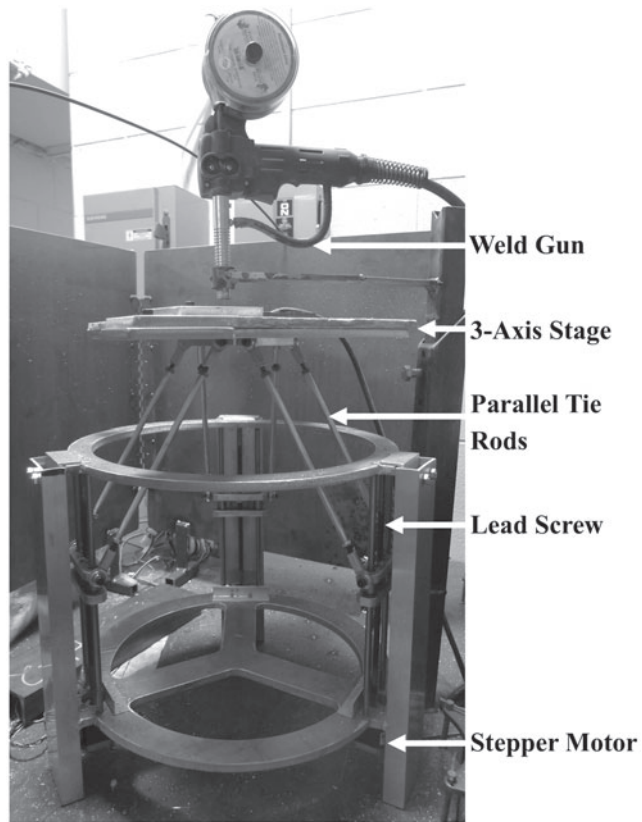


Figure 1. Labeled photograph of the three-axis stage with attached aluminum weld gun.

Mechanism	Print material	Coating	Coating thickness ( $\mu\text{m}$ )	Substrate
1	ER1100 aluminum	None	0	1100 aluminum
3	ER1100 aluminum	Aluminum oxide	18.8	1100 aluminum
3	ER1100 aluminum	Boron nitride	5.9	1100 aluminum
2	ER1100 aluminum	None	0	A36 low-carbon steel
3	ER1100 aluminum	Aluminum oxide	18.8	A36 low-carbon steel
3	ER1100 aluminum	Boron nitride	5.9	A36 low-carbon steel

The original Rostock printer had the extruder mounted on the moving end effector, whereas the three-axis stage used in this work was essentially a Rostock turned upside down, with the workpiece on the moving end effector and the “extruder” (welding gun) fixed in position above it.

During this study, welding parameters were set manually and the motion of the stage was adjusted to produce a quality bead. A quality bead was defined as a continuous line of 3D-printed material with consistent profile. Argon shield gas was used to minimize inclusions and spatter so as to produce a higher quality weld bead. Flux core wire was not utilized as it can leave a waste layer on top of the weld, making it difficult to print multiple layers.

**Details of the Three-Axis Stage**

The three-axis stage is shown in Figure 1. All of the designs for the hardware and all of the software employed are free and open-source.<sup>22</sup> The all-metal construction<sup>23</sup> minimized risk of damage due to weld spatter and heat. The drive mechanism utilized three NEMA17 stepper motors (5.5kg-cm torque) with lead screws integrated into their shafts, requiring no couplings between the motors and lead screws. The trapezoidal-threaded lead screws had a 5mm pitch and were 300mm in length. The three motors were arranged vertically on a 394 mm circle, spaced 120° apart as shown in Figure 1. In general, the three-axis stage was based upon an industrial delta robot design commonly used for pick-and-place operations, except allowing for greater movement in the z-direction.

Control was provided by an Arduino-based controller. Firmware (software resident on the printer’s microcontroller) controlled the motion of the printer, translating commands from a printer server running on a host computer. The host computer, in turn, served a web interface from which the end user was able to control stage motion, queue print jobs, and make configuration changes.

**Software Tool Chain**

RepRap 3D printers utilize stereolithography (.stl) files for the input. OpenSCAD,<sup>24</sup> a script-based open-

source CAD package, was used to develop the solid models, which were then sliced with the 3D printing software Cura<sup>25</sup> and converted into G-code. G-code provided numerical control to the stepper motors, directing them when to move and how fast to move. The metal printer interfaced with these programs using a printer server developed at Michigan Tech with a web-based interface.<sup>26</sup>

**Materials Preparation and Printing of Test Specimens**

Standard ER1100 aluminum GMAW wire, 0.030 inches (0.762mm) in diameter, was used as the weld filament, while degreased 1100 aluminum and A36 low-carbon steel were used for the print substrate materials. Three substrate release mechanisms were tested, incorporating the use of various coatings and substrate materials to modify adhesion of the 3D-printed part (Table 1). An aluminum oxide coating, approximately 18.8µm thick, was applied to the two substrate types. Coating thickness was calculated using an average mass across the surface area of the substrate. The coating was applied as a slurry prepared by mixing 100mL 95% isopropyl alcohol (BDH, Inc.) with 27g of 10µm aluminum oxide powder of 99.7% purity (Sigma-Aldrich). Mixing was performed with a magnetic stir bar for 5 minutes to ensure homogeneity. The slurry was poured onto a single

substrate at a time, held at an angle until the substrate was completely covered. The slurry was remixed between substrate coatings to minimize settling. The coated substrates were laid flat to dry for approximately 30 minutes.

An aerosol-based boron nitride coating (ZYP Coatings), approximately 5.9µm thick, was also sprayed directly onto the two substrate types. The coating thicknesses of aluminum oxide (18.8µm) and boron nitride (5.9µm) were chosen to prevent conductivity issues between the welder and substrate that might prevent arc formation and thus preclude welding. Four samples per treatment condition were prepared.

Lap shear test samples were prepared with aluminum substrate coupons (50.8×76.2×6.35mm<sup>3</sup>) butted together with a 25.4×50.8×6.35mm<sup>3</sup> print made over the butt joint (Figure 2). A sheet of 6.35-mm-thick A36 low-carbon steel was placed under the substrate plates to act as a heat sink. Relevant print parameters, including cover gas, wire feed rate, power, and slicing speed are shown in Table 2. The slicing speed is defined as the speed at which the three-axis stage, upon which the substrate rests, moves. Each test specimen was water-quenched immediately following print completion. An identical procedure was maintained for printing on A36 low-carbon steel coupons.

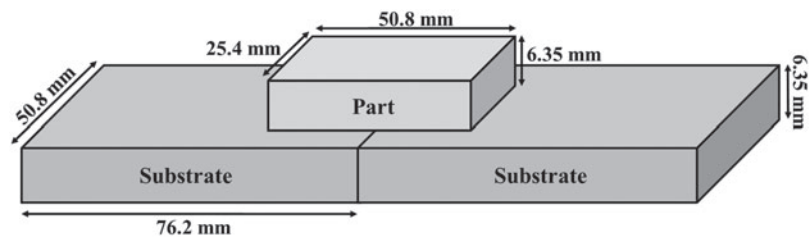


**Figure 2.** Schematic drawing of the 3D-printed aluminum lap shear test specimen.

Table 2. Print parameters for 3D printing ER1100 aluminum					
Substrate material	Weld unit voltage setting	Power (W)	Wire feed rate (in./min)	Slicing speed (mm/min)	Cover gas
ER1100 aluminum	3	854	90	180	Argon
A36 low-carbon steel	1	764	75		

### Testing and Analysis of Samples

The adhesion strength of the interface between the 3D-printed part and the substrate was quantified using a lap shear test. The substrate materials were loaded until failure by an MTS tensile load frame with a 150 kN load cell at a rate of 85  $\mu\text{m}$  per second. Failure was marked as the maximum stress required to break the printed metal coupon away from one of the substrate plates. The maximum load at failure corresponded to the strength of the interface for a given adhesion area.

### Results and Discussion

The results of the lap shear test are summarized in Figure 3. The error bars in this figure represent  $\pm 1$  standard error of the mean, which is the standard deviation normalized for sample size. Overall, it was observed that the peak breaking stress of aluminum printed on low-carbon steel was less than that of aluminum printed on aluminum, regardless of coating type. In all samples, the peak breaking stress of boron nitride-coated substrates was less than both the aluminum oxide-coated substrates and the uncoated substrates. A two-way analysis of variance (ANOVA;  $\alpha=0.05$ )

model indicated that there was a significant difference in the breaking strength between the samples printed on low-carbon steel versus aluminum. There was also a significant difference in the breaking strength between samples printed on boron nitride compared with aluminum oxide or no coating. Two-sample *t*-tests ( $\alpha=0.05$ ) confirmed these results. No deformation of the print substrate was observed.

The first substrate release mechanism, a control group, examined the adhesion strength between commercially pure aluminum printed on commercially pure aluminum. In this instance, good joining between the printed and substrate materials was observed. This result was expected because no compounds or coatings were applied to prevent adhesion.

The second substrate release mechanism attempted to exploit the formation of intermetallic phases between aluminum and low-carbon steel. Intermetallic phases form between solid solutions of different metals and are characterized as having a crystal structure that is different from each individual solid solution phase. Aluminum-iron intermetallics have been well studied, perhaps because iron is a major impurity element in

aluminum.<sup>27</sup> Chiefly, the compound  $\text{Fe}_2\text{Al}_5$  forms adjacent to the ferrous substrate and  $\text{FeAl}_3$  forms adjacent to the aluminum.<sup>28,29</sup> This formation is dominated by the diffusion of iron atoms into the liquid aluminum<sup>26</sup> and is affected by factors such as the presence of silicon in the aluminum<sup>30</sup> and carbon in the iron,<sup>31</sup> temperature, and interaction time between the aluminum and iron atoms.<sup>32</sup> While most manufacturers try to suppress the formation of aluminum-iron intermetallic compounds due to their brittle nature, here the formation of these intermetallics was encouraged to form a brittle interface between the printed part and substrate. This brittle interface may have allowed the aluminum samples to be easily removed from the low-carbon steel substrate, not only via a lap shear test but also with a hammer and chisel, exploiting the low strength of this interface.

Printing aluminum on uncoated steel worked well to prevent adhesion between the sample and the substrate. This behavior was likely the result of two factors: the formation of aluminum-iron intermetallic compounds and minimal weld penetration into the steel due to differences in thermal properties between aluminum and steel. However, future studies encompassing compositional analysis and microstructural characterization are recommended to test these hypotheses.

Both the specific heat capacity and melting temperature of aluminum are different from those of steel. For instance, the specific heat capacity of 1100 aluminum is 0.90J/(g·K), whereas the specific heat capacity of A36 low-carbon steel is 0.48J/(g·K). This indicates that more energy is required to increase the temperature of the aluminum as compared to steel. Generally, a mass of aluminum will diffuse heat more quickly than the same mass of steel due to aluminum's higher thermal conductivity. Aluminum also has a higher heat capacity allowing it to store more thermal energy before reaching temperatures yielding weld penetration in steel. These two factors allow aluminum to store more thermal energy than steel at a given temperature. This heat storage acts as an impetus to allow surface chemical reactions, such as the formation of

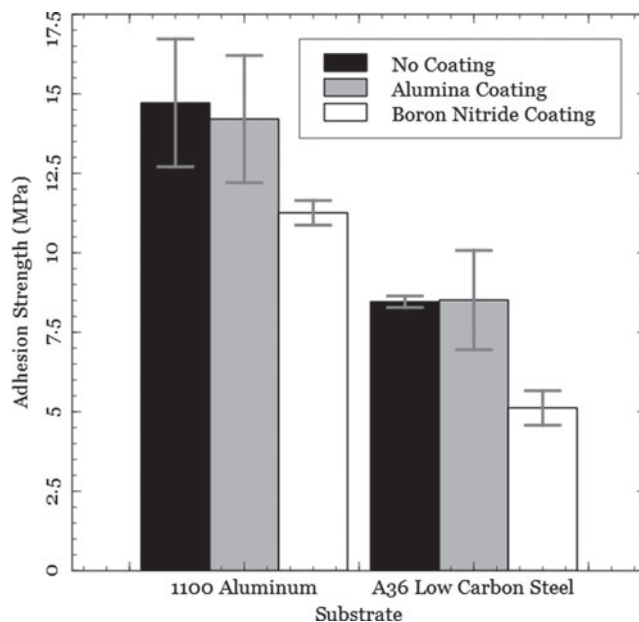


**Figure 3.** Results of the lap shear test are shown for ER1100 aluminum printed on both 1100 aluminum and A36 low-carbon steel plate, including substrates coated with aluminum oxide (alumina) and boron nitride (BN). Error bars represent  $\pm 1$  standard error.

intermetallic compounds, to occur. As described previously, a thin intermetallic layer can form a very low-strength, brittle interface between the aluminum and steel substrate that allows the aluminum to be removed from the steel with ease. As the steel remains solid at the interface due to differences in melting temperatures, there is much less mixing and diffusion of the two metals, preventing both adhesion and warping of the substrate during printing. One additional benefit of this substrate release mechanism is that it does not require additional coating materials or processes as described by the other proposed mechanisms. While the ANOVA and two-sample *t*-tests do not indicate that this mechanism provides the lowest-strength interface, it is a low-cost, no-effort method to prevent adhesion between the 3D-printed aluminum part and substrate.

The third substrate release mechanism, sacrificial aluminum oxide and boron nitride coatings, is frequently used in the metal casting industry to prevent adhesion of liquid aluminum metal to iron-based permanent molds, providing the motivation for assessing the efficacy of similar treatments on 3D metal printing substrates. Application of boron nitride coatings to a print substrate limits adhesion between 3D-printed metallic parts and metallic substrates, allowing the parts to be removed with relative ease. Even at more than triple the coating thickness, aluminum oxide (18.8 $\mu$ m coating) exhibited a higher adhesion strength than did boron nitride (5.9 $\mu$ m coating). In fact, there was no statistical difference between the adhesion strength of noncoated substrates versus aluminum oxide-coated substrates. This behavior may be due to the fact that the aluminum oxide coating did not contain any chemical binders, whereas the boron nitride coating did. These chemical binders may help the coating survive the harsh welding conditions. Some of the aluminum oxide coating may have been removed by the energy associated with rapid heating of the substrate and shield gas, limiting its ability to prevent adhesion between the molten aluminum and metallic substrate.

All of the techniques outlined in this article allow for substrate reuse, which is

both an economic and environmental benefit. Preliminary work indicated that the same substrate can be used several times. The aluminum oxide and boron nitride coatings can be scraped, sanded, or simply washed off with water to prepare the surface for reuse, an improvement over other 3D printing techniques such as laser melting and laser welding of metals, which require a sacrificial substrate.

This work enhances the value of the low-cost open-source 3D metal printer by providing a simple means for removing parts from the substrate and by permitting substrate reuse. Prototyping and manufacturing printed metal parts using this technology is not limited to just SMEs in developed regions, but also enables metal 3D printing of open-source appropriate technology<sup>33</sup> in the developing world.<sup>34</sup> Clearly, the ability to produce custom functional metal parts (e.g., bicycle components, water pump components, or small wind turbines) in a relatively isolated community would have far-reaching implications. Beyond the economic benefits, this technology may also have utility in education as assessed in work by UNESCO considering how 3D printing could be used for education in such communities.<sup>35</sup>

Evaluation of polymer-printing RepRaps demonstrated significant cost savings<sup>3</sup> and environmental benefits<sup>36</sup> as compared to conventional manufacturing methods; a similar evaluation is needed to determine the economics of this metal 3D printing method. Future work is also required to determine substrate durability and life. This will establish a reasonable substrate reuse rate as well as the effect on life cycle economics. Characterization of the printed metal part is necessary to establish compositional and mechanical properties and their relationship to the type of coating used, weld parameters, and local environment. This may be accomplished by compositional mapping, hardness measurements, and standard tensile and bend tests. The part-substrate interface also requires similar characterization to better define the mechanisms responsible for adhesion modification and to provide insight for additional manipulation of those mechanisms. In the case of printing

aluminum on uncoated low-carbon steel, additional work is necessary to establish the effect of aluminum alloy on wetting and adhesion to the substrate.

## Conclusions

This study has provided low-cost methods allowing easy removal of 3D-printed aluminum parts from readily available substrates. Printing aluminum on boron nitride-coated low-carbon steel substrates produced the weakest interfacial adhesion strength. Aluminum parts printed on uncoated low-carbon steel could also be easily removed with the benefit of not requiring application of a coating prior to printing.

## Acknowledgments

The authors would like to acknowledge P. Fraley and J. Kolacz for technical assistance, and valuable discussions with R. Gorham and America Makes. This material is based on research sponsored by Air Force Research Laboratory under Agreement Number FA8650-12-2-7230.

## Disclaimer

The U.S. Government is authorized to reproduce and distribute reprints for governmental purposes notwithstanding any copyright notation thereon. The views and conclusions contained herein are those of the authors and should not be interpreted as necessarily representing the official policies or endorsements, either expressed or implied, of Air Force Research Laboratory or the U.S. Government.

## Author Disclosure Statement

No competing financial interests exist.

## References

1. Markillie P. A third industrial revolution: Special report: Manufacturing and innovation. *The Economist* April 21, 2012.
2. Gershenfeld N. Fab: The coming revolution on your desktop—from

- personal computers to personal fabrication. Basic Books, New York, NY, 2005.
3. Wittbrodt BT, Glover AG, Laureto J, et al. Life-cycle economic analysis of distributed manufacturing with open-source 3-D printers. *Mechatronics* 2013;23:713–726.
  4. Lipson H, Kurman M. *Fabricated: The new world of 3D printing*. John Wiley & Sons, New York, NY, 2013.
  5. Khaing MW, Fuh JYH, Lu L. Direct metal laser sintering for rapid tooling: Processing and characterisation of EOS parts. *J Mater Process Technol* 2001;113:269–272.
  6. Costa Santos E, Shiomi M, Osakada K, et al. Rapid manufacturing of metal components by laser forming. *Int J Mach Tool Manu* 2006;46:1459–1468.
  7. Murr LE, Gaytan SM, Ramirez DA, et al. Metal fabrication by additive manufacturing using laser and electron beam melting technologies. *J Mater Sci Tech* 2012;28:1–14.
  8. Zhang YM, Li P, Chen Y, et al. Automated system for welding-based rapid prototyping. *Mechatronics* 2002;12:37–53.
  9. Zhao H, Zhang G, Yin Z, et al. A 3D dynamic analysis of thermal behavior during single-pass multi-layer weld-based rapid prototyping. *J Mater Process Technol* 2011;211:488–495.
  10. Wang H, Jiang W, Ouyang J, et al. Rapid prototyping of 4043 Al-alloy parts by VP-GTAW. *J Mater Process Technol* 2004;148:93–102.
  11. Wanjara P, Brochu M, Jahazi M. Electron beam freeforming of stainless steel using solid wire feed. *Mater Des* 2007;28:2278–2286.
  12. Katou M, Oh J, Miyamoto Y, et al. Freeform fabrication of titanium metal and intermetallic alloys by three-dimensional micro welding. *Mater Des* 2007;28:2093–2098.
  13. Horii T, Kirihara S, Miyamoto Y. Freeform fabrication of superalloy objects by 3D micro welding. *Mater Des* 2009;30:1093–1097.
  14. Akula S, Karanukaran KP. Hybrid adaptive layer manufacturing: An intelligent art of direct metal rapid tooling process. *Robot Comput Integr Manuf* 2006;22:113–123.
  15. Song Y-A, Park S, Choi D, et al. 3D welding and milling: Part I—a direct approach for freeform fabrication of metallic prototypes. *Int J Mach Tool Manuf* 2005;45:1057–1062.
  16. Song Y-A, Park S, Chae S-W. 3D welding and milling: Part II—optimization of the 3D welding process using an experimental design approach. *Int J Mach Tool Manuf* 2005;45:1063–1069.
  17. McGurk M, Amis AA, Potamianos P, et al. Rapid prototyping techniques for anatomical modelling in medicine. *Ann R Coll Surg Engl* 1997;79:169–174.
  18. Anzalow GC, Zhang C, Wijnen B, et al. A low-cost open-source metal 3-D printer. *IEEE* 2013;1:803–810.
  19. Jones R, Haufe P, Sells E. RepRap—the replicating rapid prototyper. *Robotica* 29;2011:177–191.
  20. ASTM Standard D1002, 2010, Standard test method for apparent shear strength of single-lap-joint adhesively bonded metal specimens by tension loading (metal-to-metal). ASTM International, West Conshohocken, PA, 2014. DOI: 10.1520/D1002-10.
  21. Reprap Org. Rostock. <http://reprap.org/wiki/Rostock> (last accessed June 24, 2014).
  22. Michigan Tech's Open Sustainability Technology Lab. Open-Source Metal 3-D Printer. [www.appropedia.org/Open-source\\_metal\\_3-D\\_printer](http://www.appropedia.org/Open-source_metal_3-D_printer) (last accessed June 24, 2014).
  23. Michigan Tech's Open Sustainability Technology Lab. Open-Source Metal 3-D Printer v2. [www.appropedia.org/MOST\\_open-source\\_metal\\_3-D\\_printer\\_v2](http://www.appropedia.org/MOST_open-source_metal_3-D_printer_v2) (last accessed June 24, 2014).
  24. OpenSCAD. [www.openscad.org](http://www.openscad.org) (last accessed June 24, 2014).
  25. Ultimaker. Software Downloads. <http://software.ultimaker.com/> (last accessed June 24, 2014).
  26. <https://github.com/mtu-most/franklin>.
  27. Belov NA, Aksenov AA, Eskin DG. Iron in aluminum alloys. Taylor & Francis, New York, NY, 2002.
  28. Bouché K, Barbier F, Coulet A. Intermetallic compound layer growth between solid iron and molten aluminum. *Mater Sci Eng A Struct Mater* 1998;249:167–175.
  29. Kobayashi S, Yakou T. Control of intermetallic compound layers at interface between steel and aluminum by diffusion-treatment. *Mater Sci Eng A Struct Mater* 2002;338:44–53.
  30. Akdeniz MV, Mekhrabov AO, Yilmaz T. The role of Si addition on the interfacial interaction in Fe-Al diffusion layer. *Scr Metall Mater* 1994;31:1723–1728.
  31. Shih TS, Tu SH. Interaction of steel with pure Al, Al-7Si and A356 alloys. *Mater Sci Eng A Struct Mater* 2007;454–455:349–356.
  32. Borrisutthekul R, Yachi T, Miyashita Y, et al. Suppression of intermetallic reaction layer formation by controlling heat flow in dissimilar joining of steel and aluminum alloy. *Mater Sci Eng A Struct Mater* 2007;467:108–113.
  33. Pearce JM. The case for open source appropriate technology. *Env Dev Sust* 2012;14:425–431.
  34. Pearce JM, Morris Blair C, Laciak KJ, et al. 3-D printing of open source appropriate technologies for self-directed sustainable development. *J Sust Dev* 2010;3:17–29.
  35. Canessa E, Fonda C, Zennaro M. Low-cost 3D printing: For science, education & sustainable development. ICTP, Trieste, Italy, 2013.
  36. Kreiger M, Pearce JM. Environmental life cycle analysis of distributed 3-D printing and conventional manufacturing of polymer products. *ACS Sust Chem Eng* 2013;1:1511–1519.

Address correspondence to:

Joshua M. Pearce  
 Department of Materials Science &  
 Engineering  
 Michigan Technological University  
 601 M&M Building  
 1400 Townsend Drive  
 Houghton, MI 49931-1295

E-mail: [pearce@mtu.edu](mailto:pearce@mtu.edu)